



Space and patchiness affects diversity–function relationships in fungal decay communities

Jade O’Leary¹ · Katie L. Journeaux¹ · Kas Houthuijs² · Jasper Engel³ · Ulf Sommer³ · Mark R. Viant³ · Daniel C. Eastwood⁴ · Carsten Müller¹ · Lynne Boddy¹

Received: 4 May 2020 / Revised: 1 October 2020 / Accepted: 5 October 2020 / Published online: 16 October 2020
© The Author(s), under exclusive licence to International Society for Microbial Ecology 2020

Abstract

The space in which organisms live determines health and physicality, shaping the way in which they interact with their peers. Space, therefore, is critically important for species diversity and the function performed by individuals within mixed communities. The biotic and abiotic factors defined by the space that organisms occupy are ecologically significant and the difficulty in quantifying space-defined parameters within complex systems limits the study of ecological processes. Here, we overcome this problem using a tractable system whereby spatial heterogeneity in interacting fungal wood decay communities demonstrates that scale and patchiness of territory directly influence coexistence dynamics. Spatial arrangement in 2- and 3-dimensions resulted in measurable metabolic differences that provide evidence of a clear biological response to changing landscape architecture. This is of vital importance to microbial systems in all ecosystems globally, as our results demonstrate that community function is driven by the effects of spatial dynamics.

Introduction

Space determines the nature of and scale over which individuals meet and interact. The characteristics of the discrete spatial habitat which an organism occupies affects individual competitive success with a bottom-up effect on population-wide colonisation, speciation and extinction [1]. There is a dynamic link between spatial ecology and competitive success where transitive (where species A

outcompetes B, which outcompetes C) communities with a strict competitive hierarchy become intransitive ($A > B$; $B > C$; $C > A$, like the game of rock–paper–scissors) when competing in a spatially more complex system [2], allowing individuals outcompeted under some scenarios to coexist with their competitors [3]. Dimensionality of habitat landscapes influences individual behaviour [4], and stochasticity of species interactions results in changes to the pool of community-produced metabolites [5], altering individual combative ability, community succession and structure between 2- and 3-dimensional landscapes [6]. Despite these findings, the mechanisms that influence stability and succession in the context of how communities occupy and exploit space are rarely adequately quantified as most ecological study systems are too complex and largely intractable. A model system is needed that allows such quantification, and understanding of how altered dynamics, coexistence and community-scale biodiversity in the context of space underpins changes in community function.

The functional diversity–area relationship, i.e., the correlation between increased habitat size and greater functional diversity, is one theory explaining how space mediates function in biodiverse communities [7]. However, the model does not account for effects of distributions and patch dynamics of species within habitats of varied area,

Supplementary information The online version of this article (<https://doi.org/10.1038/s41396-020-00808-7>) contains supplementary material, which is available to authorised users.

✉ Lynne Boddy
BoddyL@cardiff.ac.uk

¹ Cardiff School of Biosciences, Cardiff University, Cardiff CF10 3AX, UK

² Institute for Molecules and Materials, Radboud University, 6525 AJ Nijmegen, The Netherlands

³ NERC Biomolecular Analysis Facility—Metabolomics Node (NBAF-B), School of Biosciences, University of Birmingham, Birmingham B15 2TT, UK

⁴ Department of Biosciences, Swansea University, Swansea SA2 8PP, UK

yet these factors cause competitive communities to shift between hierarchical transitive and non-hierarchical intransitive relationship states [2, 8]. Non-hierarchical intransitivity is an established mechanism of coexistence [9, 10] and is thought to be associated with an intrinsically related functional-diversity mechanism [11, 12]. Wood decay fungi offer an ideal ecologically relevant model for the study of these processes as individual mycelia occupy columns of decay forming complex 3-dimensional communities in wood and, through their decomposition activities release carbon and nutrients [13]. They typically form a hierarchical community structure (tertiary/late stage colonists outcompete secondary colonists which in turn outcompete primary/earliest colonists) [14] and competitive interactions between species can be easily observed [15]. In addition to compounds that primarily function in the exploitation and decomposition of lignocellulose [16, 17], these fungi produce a plethora of potentially antagonistic compounds which function in changing territory, and differ in quantity and identity during interspecific competition [6, 18–20].

Here, we used a tractable system of wood decay fungi to quantify the impact of space on the mechanisms of coexistence and community composition, in the context of its occupation and exploitation. We compared the combative abilities of fungi in linear 2-dimensional systems and species richer 3-dimensional systems. The study system allowed more detailed analysis of community dynamics between 3-dimensional systems where fungi were dispersed in evenly spaced patches and 3-dimensional systems where the weakest member of the community occupied the same volume but as a larger adjacent patch size. Previously, our data revealed an emergent property where intransitivity promoted biodiversity in more spatially diverse 3-dimensional systems where territory was less fragmented [2]. Here, we assess the underlying mechanisms causing community stability and coexistence dynamics to change. We do this by measuring the metabolic response of an individual to changing coexistence dynamics across spatial scales. Our large-scale untargeted metabolomics and other chemical methods analysed a comprehensive network of intracellular, extracellular and gas-phase metabolic products produced during community interactions. We hypothesised that stochasticity of species would influence functional biochemical processes, and that changes to metabolites involved in pathways for resource utilisation and antagonism would alter coexistence dynamics and community composition. Spatially heterogeneous systems containing non-hierarchical communities promote biodiversity [2, 21], and here we deepen our understanding of this concept with the novel finding that space occupied alters metabolic function and coexistence, therefore, moderating the diversity–function relationship.

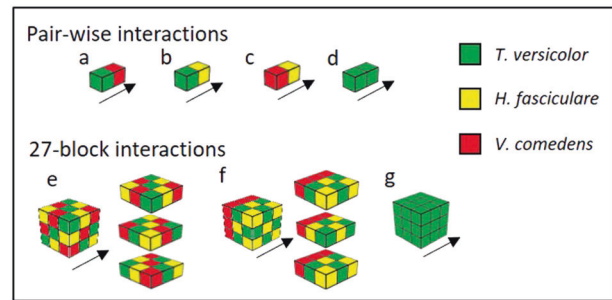


Fig. 1 Spatial distribution of species interactions. Interactions were constructed in pair-wise (a–d) and 3-dimensional 27-block (e–g) arrangements. a–d pair-wise interactions in all conceivable combinations, plus *T. versicolor* self-pairing; e dispersed cube (fungi were dispersed throughout the system and arranged so that no two blocks containing the same species had adjacent faces); f ‘wall’ distribution cubes (all fungi occupied the same total volume of wood but the adjacent territory occupied by *V. comedens* was larger; the other two competitors were arranged so that no two blocks containing the same species were adjacent); g single species, *T. versicolor* 27-block cube. Cut vessels in pair-wise interactions and rows within 27-block layers were touching so that the wood grain ran in the same parallel direction as denoted by arrows.

Methods

Experimental design and sampling

We constructed pair-wise interactions of 2 cm³ *Fagus sylvatica* (beech) blocks that had been precolonised for 12 weeks by placing on agar (5 gL⁻¹ malt extract, 15 gL⁻¹ agar; Lab M, UK) cultures of field isolates (fruit body/wood) of *Vuilleminia comedens* (strain VcWvJH1; a primary coloniser), *Trametes versicolor* (strain TvCCJH1; a secondary coloniser) and *Hypholoma fasciculare* (strain Hf DD3; a late secondary coloniser) wood decay fungi (maintained in the Cardiff University fungus culture collection), which all co-exist in nature, at 20 °C (as in [2]). Interactions were performed in all combinations including, self-pairings ($n = 10$). We also constructed 3 × 3 × 3 27-block cubes containing 9 blocks of each species. In total, 27-block cubes were arranged: (1) with all three species dispersed and no two blocks of the same species in contact ($n = 10$); (2) so that all 9 blocks of the weakest competitor, *V. comedens*, occupied an adjacent volume while the other two fungi were dispersed ($n = 10$); (3) entire 27-block assemblages containing each fungus alone (Fig. 1) [2]. Blocks in pair-wise interactions were arranged with cut vessel ends touching, and in 27-block cubes blocks were joined such that some cut vessel ends were touching but others were not, but all vessels were parallel (Fig. 1). Fungal species and specific strains were selected based on their successional order and expected combative hierarchy in the natural environment: *H. fasciculare* > *T. versicolor* > *V. comedens* [22–24] (Supplementary Table 1). Interacting combinations of wood blocks were incubated individually

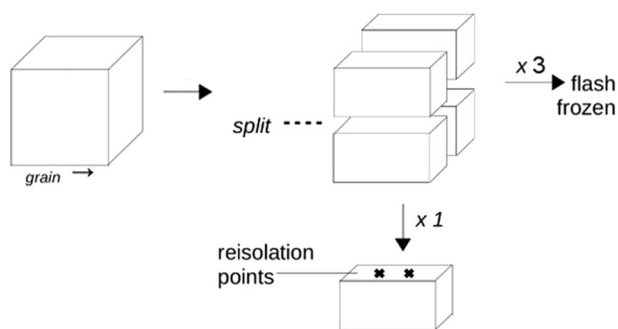


Fig. 2 Sampling and deconstruction of wood blocks. Individual blocks were split along the grain into quarters, and three of the quarters from each block were foil wrapped, flash frozen in liquid nitrogen and stored at -80°C . For the remaining quarter, two chips ($\sim 2\text{ mm}^3$) were taken from an inside face and inoculated onto 2% malt agar, then emerging mycelia identified morphologically.

at 20°C in 70 and 500 ml polypropylene pots for pair-wise and 27-block cubes, respectively, and were laid upon a layer of perlite (20 and 85 ml) containing 2 and 12 ml of water respectively which was maintained by weekly addition of water to retain the original water content, as detailed in [2]. After 1 and 28 days volatile organic compound (VOC) production was measured (described below), and we deconstructed $n = 5$ systems. Each individual block was split along the grain into quarters, and three of the quarters from each block were foil wrapped, flash frozen in liquid nitrogen and stored at -80°C . These were subsequently analysed for enzyme activity and metabolomics (see below). For the remaining quarter, two chips ($\sim 2\text{ mm}^3$) were taken from an inside face and inoculated onto 2% malt agar, incubated at 20°C , then emerging mycelia identified morphologically, to determine which species occupied the wood (Fig. 2). We removed the chip excised face from the quarter by splitting with a chisel, and determined final density as dry weight (80°C for in excess of 72 h) per fresh volume (cm^3) (blocks sampled at 28 days only), and the rate of decay estimated by comparison with density of blocks scarified ($n = 10$) at the end of the pre-colonisation period.

Overview of metabolite analysis

To quantify changes to metabolic function (antagonistic chemicals and compounds for habitat exploitation/wood decomposition) associated with different spatial dynamics in response to changing community composition, we extracted and measured: the profile of VOCs from the headspace of interactions, and the activity of 12 targeted enzymes, chosen because they are directly involved in interspecific competition [6, 19]. We also conducted ultra-high performance liquid chromatography-mass spectrometry (UHPLC-MS) metabolomics analysis. All analyses

were conducted after 1 and 28 days interactions in blocks originally colonised by *T. versicolor* ($n = 5$), and in 27-block interactions 'pseudo'-replicates representing different spatial locations within 3-dimensional cube arrays were analysed (all $n = 5$). We chose to target *T. versicolor* since the fungus has been well characterised in the past [16, 19, 25], and because it neither dominated systems (as did *H. fasciculare*) nor was it driven to near extinction (as was *V. comedens*). There were no significant differences (ANOVA: $p > 0.05$) in enzyme activity or small metabolite levels between pseudoreplicates of *T. versicolor* in 3-dimensional cubes, so we pooled activities of all pseudoreplicates for each system (therefore, $n = 15$).

VOC extraction and data preprocessing

We collected VOCs from the headspace of interactions after 1 and 28 days ($n = 3$) by inserting pots individually and lidless into a multi-purpose roasting bag (46 × 56 cm; Lakeland, UK), which was sealed for 30 min to allow VOCs to equilibrate in the headspace. Then, 500 ml headspace gas was collected onto thermodesorption (TD) tubes (Tenax TA & Sulficarb, Markes International Ltd) using an EasyVOC manual pump (Markes International Ltd, UK).

VOCs were desorbed using a TD100 TD system (Markes International Ltd, UK) with the following settings: tube desorption 10 min at 280°C , at a trap flow of 40 ml min^{-1} ; trap desorption and transfer $40^{\circ}\text{C s}^{-1}$ to 300°C , with a split flow of 20 ml min^{-1} into gas chromatograph (GC; 7890A; Agilent Technologies Inc., USA). VOCs were separated over 60 m, 0.32 mm I.D., $0.5\text{ }\mu\text{m Rx5ms}$ (Restek, UK) with 2 ml min^{-1} helium as carrier gas under constant flow conditions using the following temperature programme: 35°C for 5 min, $5^{\circ}\text{C min}^{-1}$ to 100°C , hold 5 min. Mass spectra were recorded from m/z 30 to 350 on a time-of-flight mass spectrometer (BenchTOF-dx, Markes International Ltd, UK). C8–C20 alkane standard ($0.5\text{ }\mu\text{l}$, Supelco) was loaded onto a blank TD tube as a retention standard and quality control (QC).

GC-MS data checked with MSD ChemStation software (E.02.01.1177; Agilent Technologies, Inc.) and chromatograms were deconvoluted and integrated with AMDIS (NIST11) using a custom retention-indexed mass spectral library. MS spectra from deconvolution were searched against the NIST 2011 library (Software by Stein et al., version 2.0.g, 2011). VOCs scoring $> 80\%$ in forward and backward fit and a retention index (RI) match of $+15$ were included into the custom mass spectral library as putatively identified VOCs; VOCs scoring $> 80\%$ in forward and backward fit and no RI match were included as chemical class, e.g., alkane, alkanol and recurrent components that did not show either the required mass spectral fit or RI match were added as 'unknown'. Peak list from integration

with AMDIS were aligned using the pivot function in Excel in preparation for subsequent statistical analysis.

Enzyme assays

For enzyme assays, we freeze dried the *T. versicolor* frozen blocks for 48 h (Edwards Modulyo, UK), then ground them to sawdust using a spice and coffee grinder (Wahl James Martin, UK). In total, 0.5 g of sawdust was added to 5 ml of 50 mM sodium acetate buffer and shaken overnight at 4 °C. For pair-wise interactions, *T. versicolor* blocks from all interactions and one block from its respective self-pairing were used ($n = 5$). In 27-block cubes, each fungus occupied 3 different spatial positions in both of the mixed-species assemblages, and *T. versicolor* occupied 4 spatial positions within the assemblage which it fully occupied. For each spatial position for *T. versicolor* blocks within 27-block systems (excluding the central-cube position which *T. versicolor* occupied when it was the sole occupant, as this was not represented in the mixed-species assemblages), 5 replicates were used for assays (full details in Supplementary Table 2).

The activities of the following terminal hydrolases were measured using 4 methylumbelliferol (MUF)-based substrates: β -glucosidase (EC 3.2.1.21), α -glucosidase (EC 3.2.1.20), cellobiohydrolase (EC 3.2.1.91), β -xylosidase (EC 3.2.1.37), N-acetylglucosaminidase (EC 3.2.1.30), phosphodiesterase (EC 3.1.4.1), phosphomonoesterase (EC 3.1.3.2) and arylsulfatase (EC 3.1.6.1). Briefly, substrates (40 μ l in dimethylsulfoxide) at final concentration of 500 mM were combined with three technical replicates of 200 μ l of samples (diluted 1:10) in a 96 well plate. Background fluorescence was determined by combining 200 μ l sample (diluted 1:10) with 40 μ l MUF standards. The 96 well plates were incubated at 40 °C and fluorescence recorded at 5 and 125 min using a Tecan Infinite microplate reader (Tecan, Switzerland) with an excitation wavelength of 355 nm and an emission wavelength of 460 nm. Quantitative enzymatic activities were calculated after blank subtraction based on a standard curve of MUF. One unit of enzyme activity was defined as the amount of enzyme releasing 1 nmol of MUF min^{-1} .

Laccase (phenoloxidase; EC 1.10.3.2) activity was determined by monitoring the oxidation of 2,2'-azino-bis(3-ethylbenzothiazoline-6-sulfonic acid) diammonium salt (ABTS) in citrate phosphate buffer (100 mM citrate, 200 mM phosphate, pH 5.0), by monitoring the formation of green colouration spectrophotometrically at 420 nm. Three technical replicates were performed for each sample.

Manganese peroxidase (MnP; EC 1.11.1.13) activity was determined by monitoring spectrophotometrically at 595 nm the purple colouration from oxidative coupling of 3-methyl-2-benzothialone-hydrazone hydrochloride (MBTH) and

3-(dimethyl amino)-benzoic acid (DMAB) in succinate-lactate buffer (100 mM, pH 4.5). Three technical replicates were performed for each sample. The results were corrected by activities of samples without manganese, and with ethylene diamine tetraacetate to chelate any Mn^{2+} present in the samples, allowing detection of Mn^{2+} -independent peroxidases (versatile peroxidase). The results were also corrected by activities of samples in the absence of H_2O_2 , allowing detection of oxidase (but not peroxidase) activity.

For each enzyme, $n = 3$ technical replicates were performed and enzyme activities were normalised to the protein content of each sample, which was determined using QubitTM fluorometric assays (Thermo Fisher Scientific Inc., UK).

Metabolomics analysis

As for enzyme assays, we selected blocks precolonised by *T. versicolor* ($n = 5$) upon which to perform UHPLC-MS (Supplementary Table 2). In total, 0.5 g of sawdust was added to 1666 μ l of each of H_2O , methanol and chloroform, vigorously vortexed and sonicated for 15 min (Elmasonic S150, Singen, Germany). The extracts were allowed to sit until the polar (containing H_2O and methanol) and non-polar (containing mostly chloroform) layers separated, and we then removed 1500 μ l of the upper layer containing the polar metabolite extracts. The extracts were centrifuged for 5 min at $17,000 \times g$ (Biofuge, Thermo Fisher Scientific, MA, USA), and 200 μ l of supernatant removed and dried in vacuo (Thermo Savant, NY, USA) for ca. 3 h. We then stored extracts at -80 °C until metabolomics analysis.

An intrastudy QC sample was prepared by pooling small aliquots of all samples, and the single extract was removed and dried down by centrifugation ($20,000 \times g$ for 10 min at 4 °C, Biofuge). UHPLC-MS-based metabolomics was performed (20 μ l per sample) on a Thermo Dionex Ultimate 3000 RS system with a Thermo Scientific Q Exactive Orbitrap mass spectrometer. Samples (20 μ l) were separated over a 100×2.1 mm, 1.9 μ m particles, C18 column (Thermo Hypersil Gold) at a flow rate of $400 \mu\text{l min}^{-1}$ using a 14 min linear gradient programme from 0.1% formic acid in water to 0.1% formic acid in methanol. MS acquisition started at 0.1 min, with the flow up to 0.45 min directed towards waste. We acquired data in positive ion and profile mode from m/z 100–1000 at 70,000 resolution. Samples were analysed in a controlled randomised order, with the intrastudy QC sample repeatedly analysed equidistantly between the biological samples.

Metabolomics data processing

To process the UHPLC-MS data, the Thermo.raw data files in profile mode were converted into mzML format in

centroid mode using MSConvert (Proteowizard 3.0.7665). Data were then aligned using an R (3.2.0) based XCMS and CAMERA script (both R packages [26, 27]) which resulted in a csv file intensity matrix (containing 9309 features, i.e., peaks in the mass spectra). This matrix was imported into MatLab and inserted into a direct infusion mass spectrometry SIMStitch workflow [28] where a blank filter of >2x sample over blank signal was applied, and a sample filter of peak presence of at least 50% of all samples [29]. The matrix was further processed by probabilistic quotient normalisation and subsequently missing values were imputed using K-nearest neighbour with $k = 5$. The imputed data matrix was used as an input to univariate statistics, including calculation of fold changes (FC). For multivariate statistics, a g-log transformation of the imputed data matrix was additionally applied, using an assessment of the technical variance across the repeated measurements of the intrastudy QC sample [29].

We putatively annotated UHPLC-MS features by inputting m/z values and their associated mean intensities into MI-Pack software version 2 beta [30], where metabolites were compared against the Kyoto Encyclopaedia of Genes and Genomes (KEGG) database. A set of highly significant metabolites (ANOVA: $p < 0.001$) were further searched against the KEGG database to determine possible roles within metabolic pathways.

Statistical analysis

To analyse the rate of decay and progression of interactions, we used R statistical software [31]. For each interaction, we assigned every species an individual score of combative ability, expressed as the percentage of the total system that it finally occupied. Briefly, each competitor scored between 0 and 2 for each block within a system (since two regions of every block were isolated; no outgrowth of a competitor from either isolation point scored 0, outgrowth from one isolation point scored 1, outgrowth from both isolation points scored 2). Scores for all blocks within a system were combined for each competitor individually, normalised to the number of replicates and converted to a percentage of the total system colonised. The data were analysed using a General Linear Model combined with Tukey post hoc tests, with individual block position (i.e., number of faces of that block involved in direct combat) and access to water (water was added to the perlite, as such, in 27-block interactions the layer laid on the perlite has greatest access to water) factored into the model. The rate of decay of wood in all interactions was compared using a one-way ANOVA followed by Tukey post hoc tests.

For enzyme activities, we used a one-way ANOVA with Tukey post hoc tests to compare mean activity (from five replicates), or Kruskal–Wallis tests followed by a Dunn's

test post hoc procedure when data were non-normally distributed, in R statistical software [31].

For GC-MS (VOCs) data, the entire data set was analysed by principal components analysis (PCA) to check for clustering of the QCs and, therefore, robustness of the data set (see Supplementary Fig. 1 for QC clustering), using MetaboAnalyst 3.0 [32]. We then removed QCs from the matrix, and orthogonal projection to latent structures-discriminant analysis (OPLS-DA) ($Q^2 = 0.93$, $R^2 = 0.96$), chosen for its cross-validation method which reduces false-positive results [33], was applied to the standardised binned data to determine the degree of separation between the four major sample groups: pair-wise samples 1 and 28 days after interaction set up, and 27-block samples 1 and 28 days after interaction set up. Next, we separated the data and applied OPLS-DA to pair-wise ($Q^2 = 0.57$, $R^2 = 0.61$) and 27-block ($Q^2 = 0.37$, $R^2 = 0.55$) sample groups separately. The modelled covariance and correlation were used to identify the features contributing most to the discriminant model separation, and one-way analysis of variance (ANOVA) with a 5% Benjamini–Hochberg false discovery rate (FDR) correction for multiple comparisons [34], and Tukey post hoc tests were applied to those features.

Lastly, for UHPLC-MS data we applied PCA to the g-log transformed data to explore the separation between control samples (*T. versicolor* growing alone), interaction samples and QCs. The median Relative Standard Deviation for the intrastudy QC samples was 11.15%, indicating that the MS data were of sufficiently high quality for further statistical analysis (see Supplementary Fig. 2 for QC clustering). After removing the QCs, ANOVA simultaneous components analysis (ASCA) was applied, and the model was permutation tested (5000 permutations) to determine the significance of factors (sample day, and block position within systems) [35, 36]. An additional ASCA model was tested to determine the significance of species distribution patterns within cubes, i.e., species being dispersed, *V. comedens* occupying a larger adjacent volume, or *T. versicolor* comprising the entire system, but did not include spatial location within assemblages as a factor. Pair-wise comparisons using ASCA were carried out for post hoc testing of significant effects, and the p values were adjusted for multiple testing using a 5% Bonferroni–Hochberg multiple testing correction [37]. Univariate ANOVA was applied to the whole normalised matrix with a 5% FDR correction [34] to test for significant metabolites. Finally, we determined FC between significant groups.

Network analytics

We investigated the synergy of metabolites produced by *T. versicolor* during all interactions by creating a co-occurrence Force Atlas2 [38] network analysis plot using

Sci2 [39] and Gephi [40]. Data were filtered such that only significantly abundant features (ANOVA/ASCA: adjusted $p < 0.05$) relative to the baseline were included in the analysis, and abundances of $< 10\%$ the maximum were removed from the matrix, resulting in 908 retained variables. The weighted degree of nodes was calculated, and nodes were partitioned based on their weighting to facilitate removal of those which did not cluster into a discrete module. A final network was constructed from the refined data set, with edges weighted by count of occurrence and clusters coloured by weighted degree. The average abundance of all features within a cluster was calculated, and we used a one-way ANOVA with Tukey post hoc tests with a 5% FDR correction [34] to compare mean abundance between interacting systems after 28 days, in R statistical software [31].

Results

Hierarchy and coexistence dynamics

Typical transitive hierarchy of the focus decay species, *T. versicolor*, was established in paired block interactions (Fig. 1), i.e., *H. fasciculare* $>$ *T. versicolor*, *H. fasciculare* $>$ *V. comedens*, and *T. versicolor* $>$ *V. comedens* (Fig. 3). This hierarchy reflected the general niche occupied in wood decomposition: least competitive *V. comedens* an early/primary decay species, *T. versicolor* a secondary colonising species, and *H. fasciculare* a later/tertiary decay species, the most competitive. Transitivity was also exhibited when the three fungi were dispersed throughout more spatially heterogeneous 3-dimensional systems (Fig. 1e): 15% of the original territory (defined as the relative proportion of a block occupied by a single fungus) of *T. versicolor* was captured by *H. fasciculare*, and 69% of the original territory

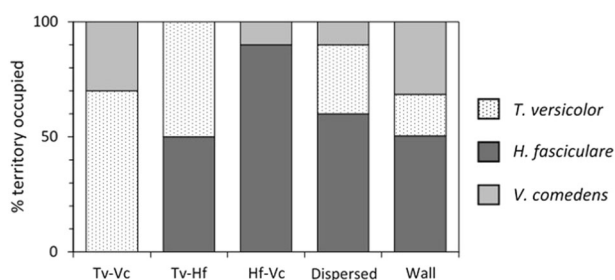


Fig. 3 Interaction progression after 28 days in pair-wise and 3-dimensional interactions. Bars show the proportion of territory occupied by each species at the end of the experiment (mean of $n = 5$, SEM = ± 12.2) in pair-wise interactions (*T. versicolor* (Tv) against *V. comedens* (Vc); *T. versicolor* against *H. fasciculare* (Hf); *H. fasciculare* against *V. comedens*), and 3-dimensional cubes in which all three species were evenly dispersed (Fig. 1e), and where *V. comedens* occupied a larger adjacent volume (Wall; Fig. 1f).

of *V. comedens* was captured by its competitors. However, when spatial dynamics within the 3-dimensional cubes were changed such that *V. comedens* occupied a larger adjacent, but same total, volume as its competitors (Fig. 1f), *V. comedens* was displaced from just 6% of its original territory, and *T. versicolor* was displaced from 46% of its original territory. The three species coexisted without *V. comedens* being driven to near extinction (within a closed community network loop) as it was when territory was patchy, which is a characteristic of an intransitive relationship (Fig. 3).

Metabolite network function

In addition to our 12 targeted enzyme assays, our untargeted analyses yielded 67 VOCs, and 2825 LCMS signals of which 1597 were putatively annotated against existing compound libraries (Supplementary Table 3). Univariate ANOVA analysis (with FDR correction of p values) and ASCA multivariate analyses provided evidence of significant differences in the quantity of individual functional metabolites from blocks originally colonised by *T. versicolor* between community systems which showed divergent coexistence dynamics. Network analysis of the detectable metabolome, VOCs and enzymes throughout all interactions (average weighted degree = 3230), revealed 10 distinct clusters of synergistic metabolites (both antagonistic and lignocellulose decaying), plus an additional 11 independently functioning compounds with a high network degree. Namely, toluene (VOC: C66), an undefined oxidase enzyme, MnP, manganese independent peroxidase (peroxidase), arylsulfatase, phosphodiesterase, and five unidentified small metabolites (Fig. 4; cluster identity Table 1).

By comparing the average abundance of individual clusters of metabolites produced in blocks precolonised by *T. versicolor* in pair-wise competitive systems, we found that production of seven clusters of antifungals was induced in significantly greater quantities when *H. fasciculare* was *T. versicolor*'s opponent, compared to three clusters when it was paired against the weaker *V. comedens*, relative to single species controls (Fig. 5). This particular response was consistent, and in 3-dimensional community interactions there was a stronger competition response shown in *T. versicolor* precolonised blocks when *V. comedens* was more combative when occupying a larger adjacent patch size (Clusters 6 and 9 were significantly more abundant (ANOVA: $p < 0.05$)), compared to when all fungi were dispersed in 3-dimensions. Cluster 6 contained the putatively annotated metabolite swainsonine, which functions in the biosynthesis pathway of piperidine- and pyridine-based antimicrobial alkaloids, and isolongifolene, a sesquiterpene with known antifungal properties, featured in Cluster 9 (Table 1). Although only putatively identified, the increased

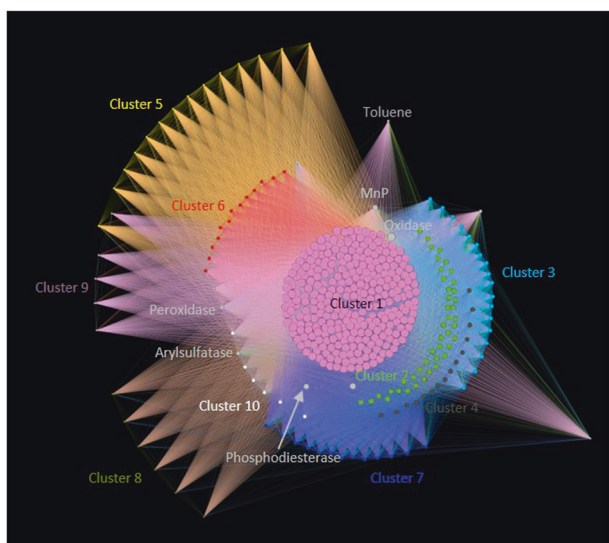


Fig. 4 Metabolic network of the full complement of significant compounds produced by *T. versicolor* throughout all interactions. Synergistic clusters of putatively annotated metabolites are clearly visualised and grouped based on their weighted degree (WD) (number of weighted edges, i.e., connections to other nodes, for a node. Average WD = 3230) and grey nodes labelled with compound names denote metabolites that did not form clusters (note that unlabelled grey nodes lack putative identifications). Clusters and their WD are detailed in Table 1. Edges are weighted by the count of occurrence of synergistic metabolites within samples, and node sizes and cluster colours represent weighted degree.

abundance of these combative/defensive compounds in *T. versicolor*-colonised blocks correlates with the increased combative ability of competitor *V. comedens* and longer coexistence of the three fungi within an intransitive relationship loop (Fig. 3).

In addition to our findings in competitive systems, we found distinct metabolic differences between 2-dimensional and more spatially complex 3-dimensional controls where *T. versicolor* was the sole occupant of these resource habitats. For example, the unclustered enzyme arylsulfatase and Cluster 10, which comprised another six similarly functioning enzymes (Table 1), were significantly more highly abundant (ANOVA: $p < 0.05$) when *T. versicolor* solely occupied a 3-dimensional cube compared to when it was solely paired in 2-dimensions (Fig. 5).

The presence of other species affected metabolic function, as for example Clusters 7 and 8, amongst others, comprising compounds such as antifungal sesquiterpenes (Table 1), were significantly more abundant (ANOVA: $p < 0.05$) when *T. versicolor* was paired in an interaction compared to when it decayed wood alone. Similarly, when we compared whole *T. versicolor* 3-d cubes with 3-d community interactions, clusters 2, 3 and 4 which contain metabolites such as ankorine and fortimicin involved in antibiotic biosynthesis pathways, were significantly more abundant (ANOVA: $p < 0.001$) in the more species-rich

systems. Within this experimental time frame the process of decomposition was not affected by spatial dynamics or species diversity (ANOVA: $p > 0.05$; Supplementary Fig. 3).

Discussion

Our results indicated that coexistence dynamics and metabolic function are directly affected by spatial occupation and patchiness of territory and can be translated into mechanistic functional processes. Furthermore, we provide evidence of a metabolic response to shifts in community structure as a result of altered connectivity. Landscape architecture changes combative mechanisms [2] and consequently may cause variation in expenditure of metabolic products between systems of varied levels of spatial heterogeneity. Community composition may be altered by a change in combative mechanisms as a result of landscape structural complexity [2], possibly due to stochastic effects within community assemblages [3] or different gaseous regimes throughout 3-dimensional structures and altered edge effects in 2-dimensions vs 3-dimensions. A study in which individuals of a community were paired against each other in artificial media [21] found negligible effects of species diversity alone on community function, but that a diverse community comprising weak competitors with high intransitivity exhibited a positive diversity–function relationship, i.e., the structure of a competitive network impacts community-level function. The more realistic complexity of the model system used in the present study revealed very different relationships: *T. versicolor* changed its mechanism of combat in systems where *V. comedens* occupied a larger adjacent volume, as clusters of metabolites functioning in the biosynthesis pathways of antagonistic antimicrobial compounds were produced in greater abundance. Presumably this emergent property was as a result of the greater combative strength of *V. comedens* (i.e., more antifungals were needed to attack the connected *V. comedens*), or as a result of a change of strategy by *H. fasciculare* which focused its attention on antagonising the now weakest competitor with whom it shared the most antagonistic fronts, *T. versicolor*, which responded to this change with increased antimicrobial compound production, or, the emergent property could have resulted from both simultaneously. Additionally, in this scenario *H. fasciculare* was able to capture some of the territory of *T. versicolor* which would result in a change to species-specific biochemical production. When *V. comedens* was dispersed it was less competitive than when connected, and connectivity of *V. comedens* altered the community dynamic such that the usually stronger competitor, *T. versicolor*, came under survival pressure. The change in mechanisms led to

Table 1 Details of a subset of putatively annotated metabolites clustered into 10 cluster sets plus unclustered metabolites, with the weighted degree (WD) of clusters given.

	Putative annotation	RI	KEGG	Pathway	Possible function
Cluster 1: WD 4089	Methyl farnesoate		C16503	Control of filamentous growth in <i>Candida albicans</i> , particularly in presence of proline and n-acetyl glucosamine	Cell signalling and growth control
	Xylobiose		C01630	Hemicellulose depolymerisation	Decomposition/sugar metabolism
	Fructoselysine		C16488	Phosphotransferase system (PTS)	Carbon metabolism
	Mannopine		C16692	ABC transporters	Cellular transport
	Decylubiquinol		C15495	Mitochondrial electron transfer chain; linked to hydroquinone biosynthesis	Lignocellulose depolymerisation
	Homocysteine		C00155	Cysteine and methionine metabolism; sulfur metabolism	Enzyme metabolism; decomposition
Cluster 2: WD 2231	(Z)-Phenylacetaldehyde oxime		C16075	Microbial metabolism in diverse environments	Metabolism of enzymes for defence
	Dethiobiotin		C01909	Biotin metabolism	Metabolism of enzymes for defence
	Alpha-Curcumene		C09649	Sesquiterpene	
	Alpha-Irone		C09690	Sesquiterpene	
	Pantetheine		C00831	Carbapenem biosynthesis; pantothenate and CoA biosynthesis	Antagonism (antimicrobial activity)
	Etidocaine		C09943	Biosynthesis of alkaloids derived from terpenoid and polyketide	Antagonism (antimicrobial activity)
	Fortimicin KL1		C17973	Biosynthesis of antibiotics	Antagonism (antimicrobial activity)
	Ankorine		C09337	Isoquinoline alkaloid biosynthesis	Antagonism (antimicrobial activity)
	Fortimicin KK1		C17974	Biosynthesis of antibiotics	Antagonism (antimicrobial activity)
	Guanine		C00242	Purine metabolism	Carbon uptake
Cluster 3: WD 1518	D-Glutamine		C00819	Metabolism of other amino acids	Defence
	N6-(delta2-Isopentenyl)-adenine		C04083	Zeatin biosynthesis	Antagonism (antimicrobial activity)
Cluster 4: WD 1892	4-Carboxy-2-hydroxy-6-methoxy-6-oxohexa-2,4-dienoate		C18345	Aminobenzoate degradation	Metabolism of enzymes for defence
	Swainsonine		C10173	Tropane, piperidine and pyridine alkaloid biosynthesis	Antagonism (antimicrobial activity)
Cluster 5: WD 331	Palmitic acid	1983	C00249	Fatty acid biosynthesis; cutin, suberine and wax biosynthesis	Antagonism (antimicrobial activity)

Table 1 (continued)

	Putative annotation	RI	KEGG	Pathway	Possible function	
Cluster 8: WD 314	5'-Phosphoribostamycin		C18004	Neomycin, kanamycin and gentamicin biosynthesis	Antagonism (antimicrobial activity)	
Cluster 10: WD 1465	Decanal	1306	C12308	Fatty acid degradation	Antagonism (antimicrobial activity)	
	α -glucosidase		EC 3.2.1.20	Galactose, starch and sucrose metabolism	Antagonism (antimicrobial activity)	
	Cellobiohydrolase		EC 3.2.1.91	Starch and sucrose metabolism	Antagonism (antimicrobial activity)	
	β -glucosidase		EC 3.2.1.21	Cyanoamino acid, starch and sucrose metabolism; Phenylpropanoid biosynthesis	Antagonism (antimicrobial activity)	
	N-acetylglucosaminidase		EC 3.2.1.30	Lipopolysaccharide neomycin, kanamycin and gentamicin biosynthesis; amino and nucleotide sugar metabolism	Antagonism (antimicrobial activity)	
Unclustered	Phosphomonoesterase		EC 3.1.3.2	Thiamine and riboflavin metabolism	Regulatory processes	
	β -xylosidase		EC 3.2.1.37	Amino and nucleotide sugar metabolism	Antagonism (antimicrobial activity)	
	Toluene	781	C01455	Degradation of aromatic compounds	Decomposition & antagonism	
	Manganese peroxidase		EC 1.11.1.13	Oxidative degradation of lignin	Antagonism (antimicrobial activity)	
	Arylsulfatase		EC 3.1.6.1	Steroid hormone biosynthesis; Sphingolipid metabolism	Antagonism (antimicrobial activity)	
	Peroxidase		C05785	Porphyrin and chlorophyll metabolism	Antagonism (antimicrobial activity)	

All putatively identified compounds were searched against the KEGG compound database, and those listed on KEGG with details of known metabolic pathways are given here along with possible function of the pathway. Retention Index (RI) is given for VOCs. See Supplementary Table 3 for full breakdown of compounds within clusters.

	Cluster1	Cluster2	Cluster3	Cluster4	Cluster5	Cluster6	Cluster7	Cluster8	Cluster9	Cluster10	M1881	C66	M2460	M2050	M1214	MnP	MUFs	Peroxidase	Oxidase	M1890	MUFpp	
TvTv : TvHf	Orange	Orange	Orange	Orange	Orange	Orange	Orange	Orange	Orange	Orange	Orange	Orange	Orange	Orange	Orange	Orange	Orange	Orange	Orange	Orange	Orange	Orange
TvTv : TvVc										Blue								Blue				Blue
TvVc : TvHf	Orange	Orange	Orange	Orange	Orange	Orange	Orange	Orange	Orange	Orange	Orange	Orange	Orange	Orange	Orange	Orange	Orange	Orange	Orange	Orange	Orange	Orange
TvCube : Dispersed	Orange	Orange	Orange	Orange	Orange	Orange	Orange	Orange	Orange	Orange	Orange	Orange	Orange	Orange	Orange	Orange	Orange	Orange	Orange	Orange	Orange	Orange
TvCube : Wall	Orange	Orange	Orange	Orange	Orange	Orange	Orange	Orange	Orange	Orange	Orange	Orange	Orange	Orange	Orange	Orange	Orange	Orange	Orange	Orange	Orange	Orange
Dispersed : Wall																						
TvTv : TvCube																						
TvVc : Dispersed		Orange	Orange	Orange	Orange	Orange	Orange	Orange	Orange	Orange	Orange	Orange	Orange	Orange	Orange	Orange	Orange	Orange	Orange	Orange	Orange	Orange
TvVc : Wall		Orange	Orange	Orange	Orange	Orange	Orange	Orange	Orange	Orange	Orange	Orange	Orange	Orange	Orange	Orange	Orange	Orange	Orange	Orange	Orange	Orange
TvHf : Dispersed																						
TvHf : Wall																						

Fig. 5 Significant differences in the average abundance of metabolic clusters (details of composition of clusters in Table 1) between interactions. Orange denotes cluster abundance is significantly higher (ANOVA: $p < 0.05$) in the interaction on the left of the colon; blue denotes significantly lower (ANOVA: $p < 0.05$) cluster abundance in the interaction on the left; and no colour denotes no

significant difference (ANOVA: $p > 0.05$) between a pair of interactions. Tv, *T. versicolor*; Vc, *V. comedens*; Hf, *H. fasciculare*; Wall, 3-dimensional cube where *V. comedens* occupied a larger adjacent volume; Dispersed, 3-dimensional cube where all three species were dispersed; TvCube, 3-dimensional cube colonised entirely by *T. versicolor* (colour figure online).

coexistence of the three species with more similar relative abundances and a closed community network loop (characteristic of intransitivity), compared to transitive community dynamics when the individuals were dispersed, where *V. comedens* was outcompeted to near extinction. It is worth noting that in natural dead wood species diversity would be greater than that presented here, and the presence of other fungal species as well as bacteria would influence interaction outcomes and, therefore, metabolism [41]. Some fungal–bacterial interactions are mutualistic [42], which could give individual fungal species a competitive advantage against their competitors, and further alter expected community hierarchies.

In the present study, production of seven substrate processing enzymes functioning in resource exploitation was boosted when spatial scale was increased from linear 2-dimensions to more heterogeneous 3-dimensions. The differences in functional metabolic processes across spatial scales, and between the more diverse community exhibiting intransitive characteristics and the transitive community is, therefore, reflective of a relationship between diversity and function that is regulated by space. The impact of the nature (space occupancy) of communities in directing community structure should be considered when looking at complex communities where outcomes are less predictable, and metabolic quantification to potentially inform predicted outcomes is, therefore, very useful.

That species diverse communities promote coexistence and positively impact community function is well known [21, 43–45]. Our results confirm this relationship between function and diversity, i.e., metabolic function changed significantly between systems with different numbers of

species (single species assemblages vs multi-species assemblages), but we also show that spatial scale and distribution of species (patch dynamics) affect metabolic function as well. While these effects were not directly translated into ecosystem services (i.e., the rate of wood decay was not significantly affected), decay in the natural environment occurs over much larger time scales than used here [46]. So it might be predicted that given a greater length of time spatial heterogeneity and species diversity would have resulted in changes to the rate of decomposition, since substrate utilisation was affected over the short time scale measured in this study. The decomposition activities of wood decay fungi determine the rate of nutrient cycling in forest ecosystems which impacts forest function [47]. The relationship between spatial dynamics, species diversity and function highlighted in our study is, therefore, a key mechanism in the release of carbon from organic substrates into the carbon cycle, which drives global change [48]. Microbial communities in every global ecosystem carry out an array of functions as important as that of wood decayers [49–51], but the effects of spatial dynamics and species diversity on these functions have not previously been measured and quantified by experimental studies. The ecologically pertinent systems presented here are pioneering in their quantitative capture of 3-dimensional spatial dynamics into the experimental study of microbial, community and landscape structural ecology, which can be adapted, reconfigured and reimagined for the study of communities with a range of interaction types (e.g., neutral, mutualistic, facilitative). Our 3-dimensional experimental design, and the finding that spatial dynamics directly impact coexistence, diversity and function, are not only translatable

to the understanding of diversity in existing microbiomes but may also provide key insights into extinctions and predictions of future ecological trends and community-level evolution.

Acknowledgements This work was supported by a Natural Environment Research Council (NERC) GW4 + DTP studentship (JO'L: NE/L002434/1), and NERC Biomolecular Analysis Facility (R8-H10-61) through an NBAF award (NBAF-977). We thank Dr. Clement Heude for training in small metabolite extraction technique.

Author contributions LB, DCE, CM and JO'L designed the experiment. JO'L and KLJ set up the experiment, KLJ, JO'L and CM analysed VOCs, JO'L analysed enzymes. JO'L, US and MRV analysed small metabolites (LCMS). JO'L, JE and KH contributed to analysis of the untargeted LCMS data, and JO'L analysed the block interactions data, enzymes data and VOC's data. JO'L, LB, DCE and CM drafted the paper, and all authors had editorial input.

Compliance with ethical standards

Conflict of interest The authors declare that they have no conflict of interest.

Publisher's note Springer Nature remains neutral with regard to jurisdictional claims in published maps and institutional affiliations.

References

- Brown JH, Maurer BA. Macroecology: the division of food and space among species on continents. *Science*. 1989;243:1145–50.
- O'Leary J, Eastwood DC, Müller CT, Boddy L. Emergent properties arising from spatial heterogeneity influence fungal community dynamics. *Fungal Ecol*. 2018;33:32–9.
- Hiscox J, Savoury M, Toledo S, Kingscott-Edmunds J, Bettridge A, Waili NA, et al. Threesomes destabilise certain relationships: multispecies interactions between wood decay fungi in natural resources. *FEMS Microbiol Ecol*. 2017;93:fix014.
- Froidevaux JSP, Zellweger F, Bollmann K, Jones G, Obrist MK. From field surveys to LIDAR: shining a light on how bats respond to forest structure. *Remote Sens Environ*. 2016;175:242–50.
- Galand PE, Pereira O, Hochart C, Christophe A, Debroas D. A strong link between marine microbial community composition and function challenges the idea of functional redundancy. *ISME J*. 2018;12:2470–8.
- O'Leary J, Hiscox J, Eastwood DC, Savoury M, Langley A, McDowell SW, et al. The whiff of decay: linking volatile production and extracellular enzymes to outcomes of fungal interactions under environmental change. *Fungal Ecol*. 2019;39:336–48.
- Karadimou EK, Kallimanis AS, Tsiripidia I, Dimopoulos P. Functional diversity exhibits a diverse relationship with area, even a decreasing one. *Sci Rep*. 2016;6:35420.
- Kolesidis DA, Boddy L, Eastwood DC, Yuan C, Fowler MS. Predicting fungal community dynamics driven by competition for space. *Fungal Ecol*. 2019;40:13–22.
- Kerr B, Riley MA, Feldman MW, Bohannan BJM. Local dispersal promotes biodiversity in a real-life game of rock-paper-scissors. *Nature*. 2002;418:171–4.
- Reichenbach T, Mobilia M, Frey E. Mobility promotes and jeopardizes biodiversity in rock-paper-scissors games. *Nature*. 2007;448:1046–9.
- Doherty JM, Callaway JC, Zedler JB. Diversity-function relationships changed in a long-term restoration experiment. *Ecol Appl*. 2011;21:2143–55.
- Song Y, Wang P, Li G, Zhou D. Relationships between functional diversity and ecosystem functioning: a review. *Acta Ecol Sin*. 2011;34:85–91.
- Bardgett RD, Freeman C, Ostle NJ. Microbial contributions to climate change through carbon cycle feedbacks. *ISME J*. 2008;2:805–14.
- Boddy L. Interspecific combative interactions between wood-decaying basidiomycetes. *FEMS Microbiol Ecol*. 2000;31:185–94.
- Hiscox J, O'Leary J, Boddy L. Fungus wars: basidiomycete battles in wood decay. *Stud Mycol*. 2018;89:117–24.
- Valášková V, Baldrian P. Estimation of bound and free fractions of lignocellulose degrading enzymes of wood rotting fungi *Pleurotus ostreatus*, *Trametes versicolor* and *Piptoporus betulinus*. *Res Microbiol*. 2006;157:119–24.
- Martinez D, Challacombe J, Morgenstern I, Hibbett D, Schmall M, Kubicek CP, et al. Genome, transcriptome, and secretome analysis of wood decay fungus *Postia placenta* supports unique mechanisms of lignocellulose conversion. *PNAS*. 2009;106:1954–9.
- Hynes J, Müller CT, Jones HT, Boddy L. Changes in volatile production during the course of fungal mycelial interactions between *Hypholoma fasciculare* and *Resinicium bicolor*. *J Chem Ecol*. 2007;33:43–57.
- Hiscox J, Baldrian P, Rogers HJ, Boddy L. Changes in oxidative enzyme activity during interspecific mycelial interactions involving the white-rot fungus *Trametes versicolor*. *Fungal Genet Biol*. 2010;47:562–71.
- El Ariebi N, Hiscox J, Scriven SA, Müller CT, Boddy L. Production and effects of volatile organic compounds during interspecific interactions. *Fungal Ecol*. 2016;20:144–54.
- Maynard DS, Crowther TW, Bradford MA. Competitive network determines the direction of the diversity-function relationship. *PNAS*. 2017;114:11464–9.
- Hiscox J, Savoury M, Vaughan IP, Müller CT, Boddy L. Antagonistic fungal interactions influence carbon dioxide evolution from decomposing wood. *Fungal Ecol*. 2015;14:24–32.
- Hiscox J, Savoury M, Müller CT, Lindahl BD, Rogers HJ, Boddy L. Priority effects during fungal community establishment in beech wood. *ISME J*. 2015;9:2246–60.
- Hiscox J, Savoury M, Johnston SR, Parfitt D, Müller CT, Rodgers H, et al. Location, location, location: priority effects in wood decay communities may vary between sites. *Environ Microbiol*. 2016;18:1954–69.
- Floudas D, Binder M, Riley R, Barry K, Blanchette RA, Henrissat B, et al. The Paleozoic origin of enzymatic lignin decomposition reconstructed from 31 fungal genomes. *Science*. 2012;336:1715–9.
- Brown M, Dunn WB, Dobson P, Patel Y, Winder CL, Francis-McIntyre S, et al. Mass spectrometry tools and metabolite-specific databases for molecular identification in metabolomics. *Analyst*. 2009;134:1322–32.
- Dunn WB, Broadhurst D, Begley P, Zelena E, Francis-McIntyre S, Anderson N, et al. Procedures for large-scale metabolic profiling of serum and plasma using gas chromatography and liquid chromatography coupled to mass spectrometry. *Nat Protoc*. 2011;6:1060–83.
- Kirwan JA, Weber RJM, Broadhurst DI, Viant MR. Direct infusion mass spectrometry metabolomics dataset: a benchmark for data processing and quality control. *Sci Data*. 2014;1:140012.
- Southam AD, Weber RJ, Engel J, Jones MR, Viant MR. A complete workflow for high-resolution spectral-stitching

- nano electrospray direct-infusion mass-spectrometry-based metabolomics and lipidomics. *Nat Protoc.* 2017;12:310.
30. Weber RJM, Viant MR. MI-Pack: increased confidence of metabolite identification in mass spectra by integrating accurate masses and metabolic pathways. *Chemom Intell Lab Syst.* 2010;104:75–82.
 31. R Core Team. R: a language and environment for statistical computing. R Foundation for Statistical Computing; 2014. <http://www.R-project.org/>.
 32. Xia J, Wishart DS. Using MetaboAnalyst 3.0 for comprehensive metabolomics data analysis. *Curr Protoc Bioinform.* 2016;55:14.10.1–91.
 33. Stelund H, Gorzias A, Persson P, Sundberg B, Trygg J. Orthogonal projections to latent structures discriminant analysis modelling on in situ FT-IR spectral imaging of liver tissue for identifying sources of variability. *Anal Chem.* 2008;80:6898–906.
 34. Benjamini Y, Hochberg Y. Controlling the false discovery rate—a practical and powerful approach to multiple testing. *J R Stat Soc B.* 1995;57:289–300.
 35. Smilde AK, Jansen JJ, Hoefsloot HC, Lamers RJ, van der Greef J, Timmerman ME. ANOVA-simultaneous component analysis (ASCA): a new tool for analyzing designed metabolomics data. *Bioinformatics.* 2005;21:3043–8.
 36. Engel J, Blanchet L, Bloemen B, van den Heuvel LP, Engelke UHF, Wevers RA, et al. Regularized MANOVA (rMANOVA) in untargeted metabolomics. *Anal Chim Acta.* 2015;899:1–12.
 37. Hochberg Y. A sharper Bonferroni procedure for multiple tests of significance. *Biometrika.* 1988;75:800–80.
 38. Jacomy M, Venturini T, Heymann S, Bastian M. ForceAtlas2, a continuous graph layout algorithm for handy network visualisation designed for the Gephi Software. *PLoS ONE.* 2014;9:e98679.
 39. Sci2 Team. Science of science (Sci2) tool. Indiana University and SciTech Strategies; 2009. <https://sci2.cns.iu.edu>.
 40. Bastian M, Heymann S, Jacomy M. Gephi: an open source software for exploring and manipulating networks. International AAAI conference on Weblogs and Social Media. Denmark: Aalborg University; 2009. pp. 361–362.
 41. Johnston SR, Boddy L, Weightman AJ. Bacteria in decomposing wood and their interactions with wood-decay fungi. *FEMS Microb Ecol.* 2016;92:fiw179.
 42. Blanchette RA, Shaw CG. Associations among bacteria, yeasts, and basidiomycetes during wood decay. *Phytopathology.* 1978;68:6317.
 43. Tilman D, Knops J, Wedin D, Reich P, Ritchie M, Siemann E. The influence of functional diversity and competition on ecosystem processes. *Science.* 1997;277:1300–2.
 44. Lambers JHR, Harpole WS, Tilman D, Knops J, Reich PB. Mechanisms responsible for the positive diversity-productivity relationship in Minnesota grassland. *Ecol Lett.* 2004;7:661–8.
 45. Hillebrand H, Matthiessen B. Biodiversity in a complex world: consolidation and progress in functional biodiversity research. *Ecol Lett.* 2009;12:1405–19.
 46. Freschet GT, Weedon JT, Aets R, van Hal JR, Cornelissen JHC. Interspecific differences in wood decay rates: insights from a new short-term method to study long-term wood decomposition. *J Ecol.* 2011;100:161–70.
 47. Hobbie SE. Effects of plant species on nutrient cycling. *Trends Ecol Evol.* 1992;7:336–9.
 48. Davidson EA, Janssens IA. Temperature sensitivity of soil carbon decomposition and feedbacks to climate change. *Nature.* 2006;440:165–73.
 49. Kandeler E, Tschirko D, Bruce KD, Stemmer M, Hobbs PJ, Bardgett RD, et al. Structure and function of the soil microbial community in microhabitats of a heavy metal polluted soil. *Biol Fertil Soils.* 2000;32:390–400.
 50. Wagner M, Loy A, Nogueira R, Purkhold U, Lee N, Daims H. Microbial community composition and function in wastewater treatment plants. *Antonie Van Leeuwenhoek.* 2002;81:665–80.
 51. Tremaroli V, Bäckhed F. Functional interactions between the gut microbiota and host metabolism. *Nature.* 2012;489:241–9.